Competition between Hund's coupling and Kondo effect in a one-dimensional extended periodic Anderson model

I. Hagymási, J. Sólyom, and Ö. Legeza
Strongly Correlated Systems "Lendület" Research Group, Institute for Solid State Physics and Optics, MTA Wigner Research Centre for Physics, Budapest H-1525 P.O. Box 49, Hungary
(Received 25 March 2015; revised manuscript received 2 June 2015; published 6 July 2015)

We study the ground-state properties of an extended periodic Anderson model to understand the role of Hund's coupling between localized and itinerant electrons using the density-matrix renormalization group algorithm. By calculating the von Neumann entropies we show that two phase transitions occur and two new phases appear as the hybridization is increased in the symmetric half-filled case due to the competition between Kondo effect and Hund's coupling. In the intermediate phase, which is bounded by two critical points, we found a dimerized ground state, while in the other spatially homogeneous phases the ground state is Haldane-like and Kondo-singlet-like, respectively. We also determine the entanglement spectrum and the entanglement diagram of the system by calculating the mutual information thereby clarifying the structure of each phase.

DOI: 10.1103/PhysRevB.92.035108 PACS number(s): 71.10.Fd, 71.27.+a, 75.30.Mb

I. INTRODUCTION

The colossal magnetoresistance observed in certain manganites has attracted much attention in condensed matter physics [1,2]. Typically perovskite manganites, for example $La_{2/3}Ca_{1/3}MnO_3$, exhibit this enormous enhancement of the magnetoresistance [1]. It is now generally accepted that the colossal magnetoresistance originates from the strong correlation between electrons, namely the double exchange and superexchange interactions, Jahn-Teller effect, etc. play an important role, although this phenomenon is far from being understood [3]. In these compounds due to the crystal field, the fivefold degenerate d orbitals are split into twofold degenerate (e_g) and threefold degenerate (t_{2g}) orbitals which are coupled to each other via Hund's coupling. The electrons in the e_g orbitals are delocalized while the t_{2g} electrons are localized [4]. To understand the compounds in question, it is crucial to investigate models with more than one orbital. Hybridization between different orbitals is claimed to be important also in other compounds like $Ca_{2-x}Sr_xRuO_4$ [5]. This compound exhibits several remarkable phenomena like orbital-selective Mott transition [6] or heavy-fermion [7] behavior as the chemical concentration or temperature is varied. To account for these effects, multiorbital systems have been the focus of intensive research recently [8–12]. Our purpose here is to consider further the properties of multiorbital systems.

The starting point of our investigations is the periodic Anderson model [13–15], which is a minimal model with two kinds of electrons:

$$\begin{aligned}\mathcal{H}_{\mathrm{PAM}} = &\sum_{\boldsymbol{k}\sigma} \varepsilon_{\boldsymbol{k}} \hat{c}^{\dagger}_{\boldsymbol{k}\sigma}\hat{c}_{\boldsymbol{k}\sigma} + \varepsilon_f \sum_{j\sigma} \hat{f}^{\dagger}_{j\sigma}\hat{f}_{j\sigma} \\ &+ \sum_{j\boldsymbol{k}\sigma} (V_{\boldsymbol{k}} e^{-i\boldsymbol{k}\boldsymbol{R}_j} \hat{f}^{\dagger}_{j\sigma}\hat{c}_{\boldsymbol{k}\sigma} + V^{*}_{\boldsymbol{k}} e^{i\boldsymbol{k}\boldsymbol{R}_j} \hat{c}^{\dagger}_{\boldsymbol{k}\sigma}\hat{f}_{j\sigma}) \\ &+ U_f \sum_j \hat{n}^{(f)}_{j\uparrow}\hat{n}^{(f)}_{j\downarrow}. \end{aligned} \tag{1}$$

Here $\hat{c}^{\dagger}_{\boldsymbol{k}\sigma}$ ($\hat{c}_{\boldsymbol{k}\sigma}$) creates (annihilates) an electron with spin σ in a wide band with dispersion curve $\varepsilon_{\boldsymbol{k}}$. This band will be described in the tight-binding approximation with nearest-neighbor overlap only. Furthermore, $\hat{f}^{\dagger}_{j\sigma}$ ($\hat{f}_{j\sigma}$) creates (annihilates) localized electrons at site j with spin σ and the corresponding particle number operator is $\hat{n}^{(f)}_{j\sigma} = \hat{f}^{\dagger}_{j\sigma}\hat{f}_{j\sigma}$. They can be mixed to the states of the wide band by the matrix element $V_{\boldsymbol{k}}$. When the states of the wide band are written in a real-space representation, this mixing is in general nonlocal, however, we neglect its $\boldsymbol{k}$ dependence in the following $V_{\boldsymbol{k}} = V$. The Coulomb interaction between localized electrons is U_f, and their on-site energy is ε_f.

Our goal is to study the interactions between the two kinds of electrons, whose general form in momentum space can be written as

$$\mathcal{H} = \mathcal{H}_{\mathrm{PAM}} + \frac{1}{2V} \sum_{\substack{\boldsymbol{k}\boldsymbol{k}'\boldsymbol{q} \\ \sigma\sigma'}} U_{\sigma\sigma'}(\boldsymbol{q}) c^{\dagger}_{\boldsymbol{k}+\boldsymbol{q}\sigma} f^{\dagger}_{\boldsymbol{k}'-\boldsymbol{q}\sigma'} f_{\boldsymbol{k}'\sigma'} c_{\boldsymbol{k}\sigma}, \tag{2}$$

which is visibly nonlocal in real space for a general $U_{\sigma\sigma'}(\boldsymbol{q})$ interaction. In what follows we consider only on-site interactions between the two kinds of electrons, taking into account the interorbital Coulomb interaction and the direct exchange between them, described by the rotationally invariant Kanamori Hamiltonian [16]. In addition to that we also include an on-site repulsion for the delocalized electrons. To write the Hamiltonian in a convenient form, we use the real-space representation for the creation and annihilation operators of the electrons in the wide band ($\hat{c}^{\dagger}_{j\sigma}, \hat{c}_{j\sigma}$), then the total Hamiltonian becomes

$$\begin{aligned}\mathcal{H} = \mathcal{H}_{\mathrm{PAM}} &+ U_c \sum_j \hat{n}^{(c)}_{j\uparrow}\hat{n}^{(c)}_{j\downarrow} + \sum_{j\sigma\sigma'} (U_{cf} - J\delta_{\sigma\sigma'}) \hat{n}^{(c)}_{j\sigma}\hat{n}^{(f)}_{j\sigma'} \\ &- J \sum_j [(\hat{c}^{\dagger}_{j\uparrow}\hat{c}_{j\downarrow}\hat{f}^{\dagger}_{j\downarrow}\hat{f}_{j\uparrow} + \hat{c}^{\dagger}_{j\uparrow}\hat{c}^{\dagger}_{j\downarrow}\hat{f}_{j\uparrow}\hat{f}_{j\downarrow}) + \mathrm{H.c.}], \end{aligned} \tag{3}$$

where U_c is the Coulomb repulsion within the wide band, U_{cf} denotes the local interaction between the two kinds of electrons, and J is the Hund's coupling. It is worth noting that one can always diagonalize the bilinear part of the Hamiltonian obtaining two orthogonal bands. However, in that case the intraorbital interaction becomes nonlocal in terms of the original operators [17].

The role of the term U_c and U_{cf} has been examined in several papers [18–25]. It has been shown that U_c leads to significant enhancement of the effective mass in the Kondo regime, while U_{cf} causes critical valence fluctuations in the mixed valence regime and can lead to charge ordering in infinite spatial dimensions. The full Hamiltonian in Eq. (3) including J has also been investigated thoroughly by dynamical mean-field theory (DMFT) in infinite spatial dimensions [9,16,26,27], and it was revealed how the Kondo and Mott insulating states compete with the metallic state in the half-filled case if the system is assumed to be paramagnetic [26]. It turned out, however, that magnetic long-range order can also be present in the model, namely two types of antiferromagnetic order emerge beside the Kondo insulating state [27]. The occurrence of these phases originates from the competition between Hund's coupling and Kondo effect. While the former one aligns the spins of localized and itinerant electrons ferromagnetically at a given site, the latter one tries to screen the localized spins by forming singlets with the itinerant electrons. It has also been discussed how the hybridization affects the orbital-selective Mott localization emerging in two-orbital Hubbard models [16].

Since the DMFT approach completely neglects the spatial fluctuations, which is only valid in infinite dimensions, it is necessary to investigate low-dimensional systems where quantum fluctuations are known to be much stronger. Our main goal in this paper is to explore the one-dimensional behavior of the Hamiltonian in Eq. (3). In earlier papers it has been shown [25,28,29] that there is no quantum phase transition in one dimension in the absence of the Hund's coupling in contrast to the infinite dimensional case. The competition between the Hund's coupling and the Kondo effect may lead to the appearance of quantum phase transitions and unexpected phases even if true long-range order cannot be present in one dimension.

We apply the density-matrix renormalization-group method (DMRG) [30–34], which is a powerful tool to find the ground state and to determine the correlation functions. Further advantage of the DMRG method is that we can easily determine the von Neumann entropies [35–40] of single and multisite subsystems, without the need to calculate excited states, which is in general difficult near a critical point, and their anomalies can be used to detect quantum phase transitions [41–44].

In our DMRG calculation we applied the dynamic block-state selection algorithm [45,46] in which the threshold value of the quantum information loss χ is set *a priori*. We have taken $\chi = 3 \times 10^{-6}$. A maximum of 2000 block states is needed to achieve this accuracy, and the truncation error was in the order of 10^{-7}. Such low value of χ is necessary in order to obtain "smooth" data sets close to critical points. We investigated chains up to a maximum length $L = 120$ with open boundary conditions and performed eight sweeps.

The setup of the paper is as follows. In Sec. II we define the von Neumann entropies of various subsystems used in our analysis, and the mutual information [38,47,48]. In Secs. III A, III B, and III C we discuss the properties of the phases occurring in the model using the mutual information and the eigenvalue spectra of the two-site density matrices. In Sec. III D we discuss the differences between the phase diagram obtained in the DMFT and for the one-dimensional model. Finally, in Sec. IV our conclusions are presented.

II. VON NEUMANN ENTROPIES

The von Neumann entropies of different subsystems are known to exhibit anomalies near critical points [39,41,42]. We examined the one-site s_i, two-site s_{ij} entropies and the block entropy which is the entropy of the subsystem containing sites from 1 to $L/2$. These quantities can be obtained from the appropriate reduced density matrices [35,36,39]. The entropy of a single site can be obtained as

$$s_i = -\mathrm{Tr}\rho_i \ln \rho_i, \tag{4}$$

where ρ_i is the reduced density matrix of site i, which is derived from the density matrix of the total system by tracing out the configurations of all other sites. We also define the entropies corresponding to the two types of electrons at a site $(s_i^{(c)}, s_i^{(f)})$ in the following way:

$$s_i^{(c)} = -\mathrm{Tr}\rho_i^{(c)} \ln \rho_i^{(c)}, \tag{5}$$

$$s_i^{(f)} = -\mathrm{Tr}\rho_i^{(f)} \ln \rho_i^{(f)}, \tag{6}$$

where $\rho_i^{(c)}$ ($\rho_i^{(f)}$) is obtained by performing an additional trace over the remaining f (c) degrees of freedom at site i. The two-site entropy is written as

$$s_{ij} = -\mathrm{Tr}\rho_{ij} \ln \rho_{ij}, \tag{7}$$

where ρ_{ij} is the two-site reduced density matrix of sites i and j. We can also introduce the partial two-site entropies for type a electrons on site i and type b electrons on site j:

$$s_{ij}^{(ab)} = -\mathrm{Tr}\rho_{ij}^{(ab)} \ln \rho_{ij}^{(ab)}, \quad a,b \in \{c,f\}, \tag{8}$$

where $\rho_{ij}^{(ab)}$ is derived from ρ_{ij} by tracing out the states of the other electrons. The mutual information [49–51] which measures the entanglement between sites i and j can be obtained from

$$I_{ij} = s_i + s_j - s_{ij}, \tag{9}$$

while the mutual information between a and b type electrons on sites i and j is defined as

$$I_{ij}^{(ab)} = s_i^{(a)} + s_j^{(b)} - s_{ij}^{(ab)}, \tag{10}$$

which measures all correlations both of classical and quantum origin between a and b type electrons on sites i and j. In what follows we refer to $I_{ij}^{(ab)}$ as the entanglement between these components. Finally, the block entropy is defined as

$$s(L/2) = -\mathrm{Tr}\rho_A \ln \rho_A, \tag{11}$$

where A denotes the subsystem which contains the sites from 1 to $L/2$. In contrast to the one- or two-site entropies, which have a finite upper bound, the block entropy grows as $O(\ln L)$ for one-dimensional critical systems [36,37].

III. RESULTS

In what follows we consider the half-filled case and nearest-neighbor hopping between delocalized electrons

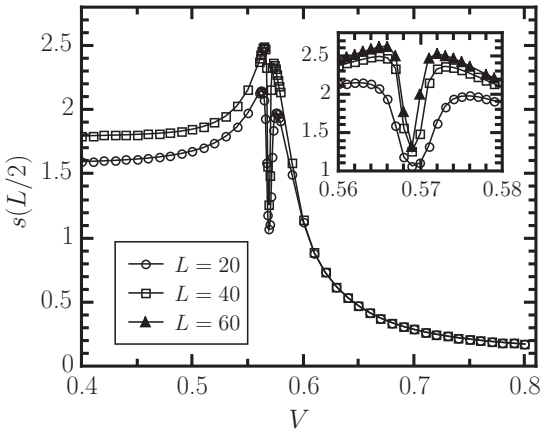

FIG. 1. The block entropy $s(L/2)$ as a function of hybridization for different chain lengths and $J/U = 0.1$. The lines are guides to the eye.

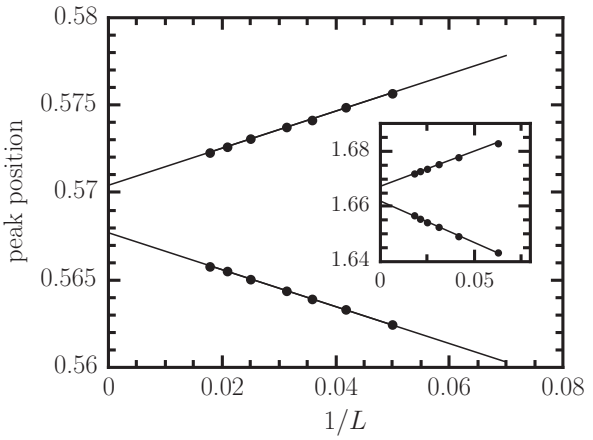

FIG. 2. The main figure shows the finite-size scaling of the peaks occurring in the block entropy for $J/U = 0.1$, while the inset shows the same for $J/U = 0.3$. The lines are the best linear fits to the data. The estimated error is comparable to the size of the symbols.

$\varepsilon(k) = -2t\cos k$, and use the half bandwidth $W = 2t$ as the energy scale of the system and set $\varepsilon_f = 0$. For simplicity we assume $U_c = U_f = U$ and $U = U_{cf} + 2J$. In the absence of Hund's coupling the ground state in one dimension is either a collective singlet or consists of less entangled local Kondo singlets depending on the values of Coulomb interactions and the hybridization [25]. There is no quantum phase transition between these phases, just a smooth crossover separates them. To examine the effect of the Hund's coupling, first we consider what happens for a finite Hund's coupling, namely for $J/U = 0.1$ and 0.3, with $U = 4W$ as the hybridization is varied.

First, we investigate the block entropy of one half of the chain. This quantity is a smooth function of V for any U when $J = 0$. For any finite J, however, two peaks appear in the block entropy as can be seen in Fig. 1 for different chain lengths for a fixed value of $J/U = 0.1$, where the two peaks are around $V/W = 0.57$. It is clearly observed that the height of the peaks increases as the chain length is increased. We know that maxima in the block entropy can be attributed to quantum critical points [39] if they evolve into anomalies in the thermodynamic limit. Two peaks may indicate the existence of two phase transitions separating three different phases. To check if it is indeed the case, one has to show that the peaks remain separated and do not merge in the thermodynamic limit. The finite-size scaling of the position of the peaks is shown in Fig. 2. We could treat systems with $L = 60$ sites near the critical points due to the high value of the block entropy. To determine the positions of the maxima accurately we used a cubic spline interpolation. Figure 2 shows that the position of the peaks as a function of $1/L$ can be fitted well with a linear function and the phases remain separated in the thermodynamic limit having positions

$$\begin{aligned} V_1^{\rm cr}/W &= 0.5677(0), \\ V_2^{\rm cr}/W &= 0.5704(1) \end{aligned} \tag{12}$$

for $J/U = 0.1$. As a remark we mention that to estimate the error of the data points in Fig. 2 we use the following analysis. The quantum information loss was *a priori* set to $\chi = 3 \times 10^{-6}$. Therefore, the relative error of the ground state energy is estimated to be of the same order of magnitude, $\delta E_{\rm rel} \sim 10^{-6}$. Since the ground state energies are of the order of $E \sim 10^2$, the absolute error of the energies is of the order of $\delta E_{\rm abs} \sim 10^{-4}$, so the error of the block entropy can be expected to be not larger than $\delta S_{\rm abs} \sim 10^{-4}$. The block entropy values near the critical points were sampled with an equidistant step 5×10^{-4} (for better visibility not all are shown in Fig. 1). The error of the spline fit is also expected to be 10^{-4}. All in all the overall error is expected to be 10^{-4}, which is comparable to the size of the symbols in Fig. 2.

We repeated the same calculation for other values of J/U. Our results indicate that two separate peaks are present in the block entropy for any finite J. The distance of the peaks is shown in Table I for two values of J/U for different chain lengths. It is clear that their distance grows as J is increased, furthermore, the critical values of V are also shifted towards larger values. In what follows we analyze the ground state properties of each phase for $J/U = 0.1$ using the mutual information and correlation functions to check if the peaks indeed separate different phases.

A. The Kondo singlet phase for $V_2^{\rm cr} < V$

First, we consider what happens for large hybridization where the effect of Hund's coupling is expected to be small compared to that of hybridization and the Coulomb interaction and the properties of the $J = 0$ model are expected to be recovered. We examine how the individual system components are entangled to each other using the mutual information. We have seen already in Fig. 1 that for large values of

TABLE I. The distance of the peaks of the block entropy for several chain lengths and J/U ratios. The extrapolation was performed using chains up to $L = 60$.

J/U	$L = 16$	$L = 24$	$L \to \infty$
0.1	0.016	0.011	0.0027(1)
0.3	0.040	0.028	0.006(8)

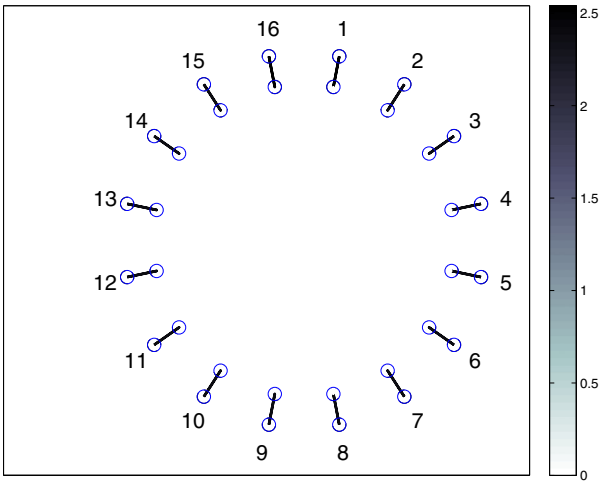

FIG. 3. (Color online) Schematic view of all components of the mutual information ($I_{ij}^{(cc)}$, $I_{ij}^{(cf)}$, $I_{ij}^{(ff)}$) for $V/W = 0.8$ and $L = 16$. The numbers are the site indices. The inner and outer circles denote type f (localized) and type c (itinerant) electrons.

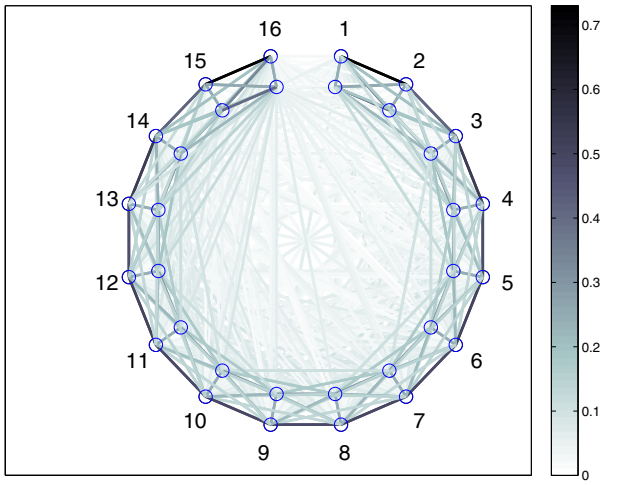

FIG. 4. (Color online) The same as in Fig. 3, but for $V/W = 0.3$.

the hybridization the block entropy decreases rapidly, which indicates a less entangled state. This is the case indeed, as is seen in the entanglement map in Fig. 3. We can see that very strong on-site entanglement appear, while the one-particle states on different sites are hardly entangled to each other. To describe the physical origin of this difference in the entanglement within a site and between neighboring sites we calculated the eigenvalues ($\omega_\gamma, \gamma = 1,\ldots,16$) of the two-site density matrix $\rho_{ij}^{(ab)}$ and the corresponding eigenfunctions. From $\rho_{L/2,L/2}^{(cf)}$ we found that for $V/W = 0.8$ one of its eigenvalues is larger by two orders of magnitude than the others and the corresponding eigenvector is

$$\phi_{L/2,L/2}^{(cf)} = 0.5574\big(|\uparrow\rangle_{L/2}^{(c)}|\downarrow\rangle_{L/2}^{(f)} - |\downarrow\rangle_{L/2}^{(c)}|\uparrow\rangle_{L/2}^{(f)}\big) + 0.4350\big(|\uparrow\downarrow\rangle_{L/2}^{(c)}|0\rangle_{L/2}^{(f)} + |0\rangle_{L/2}^{(c)}|\uparrow\downarrow\rangle_{L/2}^{(f)}\big). \quad (13)$$

Here $|0\rangle_i^a$, $|\uparrow\rangle_i^a$, $|\downarrow\rangle_i^a$, $|\uparrow\downarrow\rangle_i^a$ denote the four possible states of electron type a on site i. We can see that strong on-site singlets are formed between localized and delocalized electrons, which we may refer to as Kondo singlets, since this is the consequence of the enhanced Kondo effect. The entanglement between nearest-neighbor sites is smaller by two orders of magnitude than the on-site entanglement between localized and delocalized electrons. Therefore, the ground state is almost a product state. Since the eigensystem of $\rho_{L/2,L/2+1}^{(cc)}$ and $\rho_{L/2,L/2+1}^{(ff)}$ is quantitatively the same, we consider only the former one. The eigenfunction belonging to the most significant eigenvalue of $\rho_{L/2,L/2+1}^{(cc)}$ reads

$$\phi_{L/2,L/2+1}^{(cc)} = 0.6900\big(|\uparrow\rangle_{L/2}^{(c)}|\downarrow\rangle_{L/2+1}^{(c)} - |\downarrow\rangle_{L/2}^{(c)}|\uparrow\rangle_{L/2+1}^{(c)}\big) + 0.1545\big(|\uparrow\downarrow\rangle_{L/2}^{(c)}|0\rangle_{L/2+1}^{(c)} + |0\rangle_{L/2}^{(c)}|\uparrow\downarrow\rangle_{L/2+1}^{(c)}\big), \quad (14)$$

that is, the nearest neighbor coupling between the spins is antiferromagnetic. We checked that the mutual information components have their bulk values at $L = 16$ already, which is due to the hardly entangled ground state. Indeed, the properties of this phase agree with the known behavior of the conventional periodic Anderson model for large hybridization.

B. The Haldane-like phase for $V < V_1^{cr}$

A new phase is expected to appear for small hybridization, where J dominates. Here we discuss the properties of the phase emerging for $V < V_1^{cr}$ using the mutual information. The entanglement diagram containing all types of the mutual information is shown in Fig. 4 for $V/W = 0.3$. One can see that the strongest entanglement is developed between neighboring delocalized electrons and moderately strong entanglement is present between more distant sites.

First, we consider how the eigenvalue spectrum looks like for $\rho_{L/2,L/2}^{(cf)}$ and $L = 16$. We found that one of its eigenvalues is threefold degenerate and larger by an order of magnitude than the others. Its value is very close to 1/3 and the three corresponding eigenfunctions $\phi_{L/2,L/2}^{(cf),\gamma}$ $\gamma = 1,2,3$ read

$$\begin{aligned}\phi_{L/2,L/2}^{(cf),1} &= |\uparrow\rangle_{L/2}^{(c)}|\uparrow\rangle_{L/2}^{(f)},\\ \phi_{L/2,L/2}^{(cf),2} &= \frac{1}{\sqrt{2}}\big(|\uparrow\rangle_{L/2}^{(c)}|\downarrow\rangle_{L/2}^{(f)} + |\downarrow\rangle_{L/2}^{(c)}|\uparrow\rangle_{L/2}^{(f)}\big), \quad (15)\\ \phi_{L/2,L/2}^{(cf),3} &= |\downarrow\rangle_{L/2}^{(c)}|\downarrow\rangle_{L/2}^{(f)}.\end{aligned}$$

That is, the electrons on the same site are in a state where the $S = 1$ triplet components have the largest weights.

As a next step we examine the entanglement between nearest-neighbor sites. Since the eigensystems of $\rho_{L/2,L/2+1}^{(cc)}$, $\rho_{L/2,L/2+1}^{(cf)}$, and $\rho_{L/2,L/2+1}^{(ff)}$ are quantitatively very similar, we only present results for $\rho_{L/2,L/2+1}^{(ff)}$. The eigenfunction corresponding to the most significant eigenvalue is

$$\phi_{L/2,L/2+1}^{(ff)} = 0.7071\big(|\uparrow\rangle_{L/2}^{(f)}|\downarrow\rangle_{L/2+1}^{(f)} - |\downarrow\rangle_{L/2}^{(f)}|\uparrow\rangle_{L/2+1}^{(f)}\big) + 0.0014\big(|\uparrow\downarrow\rangle_{L/2}^{(f)}|0\rangle_{L/2+1}^{(f)} + |0\rangle_{L/2}^{(f)}|\uparrow\downarrow\rangle_{L/2+1}^{(f)}\big), \quad (16)$$

which means that the entanglement between the neighboring sites results mainly from the singlet formation. Furthermore, we investigated how the mutual information components scale

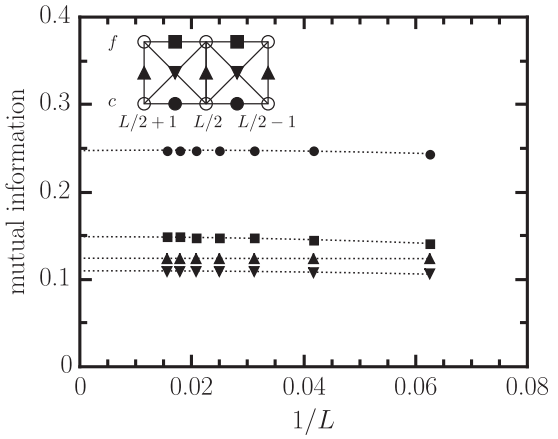

FIG. 5. The finite-size scaling of the mutual information for $V = 0.3W$. The dotted lines are quadratic polynomial fits to the data. The inset drawing denotes a segment of the middle of the chain, the circles denote the type c and type f electrons on a given site, while the symbols denote the bonds shown in the main plot.

as the system size is increased. This is shown in Fig. 5. It is obviously seen that the bonds hardly change as the chain length becomes larger. The extrapolation was performed using a quadratic polynomial:

$$I_{ij}^{(ab)}(L) = I_{ij}^{(ab)} + A/L + B/L^2, \tag{17}$$

where $I_{ij}^{(ab)}$, A, and B are free parameters.

This confirms that the spins are aligned ferromagnetically within a site, but they couple antiferromagnetically between nearest-neighbor sites. The former one is a consequence of the strong Hund's coupling which prefers parallel alignment of the spins, while the latter one is due to the RKKY interaction mediated by the conduction electrons. The same structure was confirmed for $V = 0$. These findings suggest that the model in this regime can be considered as an $S = 1$ Heisenberg chain with antiferromagnetic nearest-neighbor coupling, therefore this is a Haldane-like phase. The ground state is a singlet, however, in the thermodynamic limit the ground state of an open chain becomes degenerate with the first $S = 1$ excited state due to the end spins. This is a well-known property of the Haldane phase [52].

C. The dimerized phase for $V_1^{cr} < V < V_2^{cr}$

Finally, we examine the properties of the narrow intermediate phase, whose appearance is indicated by the analysis of the block entropy. Using the tools applied in the previous subsections we examine the spatial structure of the ground state. The entanglement map shown in Fig. 6 is drastically different from that in the previous phase. It is clearly seen that strong and weak bonds alternate along the chain, which suggests a spatially inhomogeneous, dimerized ground state. Before investigating the physical processes that contribute to the creation of the strong entanglement, it is important to check if the dimerization remains finite in the thermodynamic limit. We can introduce two types of order parameters for the

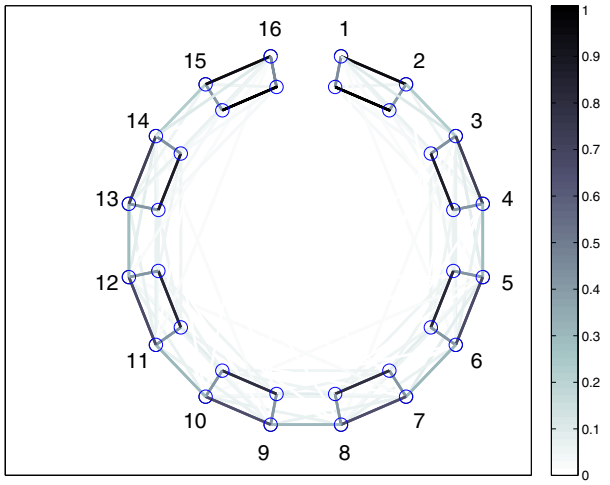

FIG. 6. (Color online) The same as in Fig. 3, but for $V/W = 0.569$.

dimerization:

$$D_1^{(a)}(V) = \lim_{L\to\infty} \left| I_{L/2,L/2+1}^{(aa)}(V) - I_{L/2-1,L/2}^{(aa)}(V) \right|, \tag{18}$$

$$D_2(V) = \lim_{L\to\infty} |s(L/2,V) - s(L/2+1,V)|. \tag{19}$$

Since $D_1^{(a)}(V)$ is a local quantity, we expect that it is less sensitive to the boundary effects. It requires, however, the calculation of several correlation functions, and their computation time scales as L^2 which can be computationally demanding. The quantity in Eq. (19) is computationally less demanding, but since the block entropy is a nonlocal quantity its convergence to the bulk value may be slower. Instead of showing $D_1^{(a)}(V)$ directly, we plot the individual values of the mutual information components ($I_{L/2,L/2+1}^{(aa)}$, $I_{L/2-1,L/2}^{(aa)}$) and investigate their size dependence. In this case we could consider chains up to $L = 120$, since in the intermediate phase the block entropy has a much lower value than near the critical points and its low value also indicates a less entangled ground state as expected for a dimerized phase. This is shown in Fig. 7. In Fig. 7 we used a quadratic polynomial, Eq. (17),

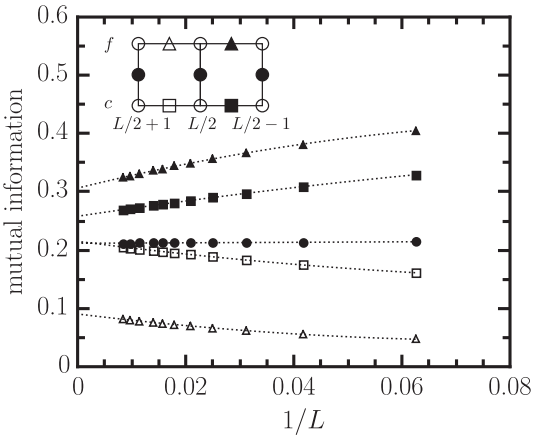

FIG. 7. The same as in Fig. 5, but for $V/W = 0.569$.

TABLE II. The extrapolated dimerization order parameters for different types of fits at $V/W = 0.569$.

Type of fit	$D_1^{(c)}(V)$	$D_1^{(f)}(V)$	$D_2(V)$
Quadratic	0.043(0)	0.215(9)	0.32(4)
Power law	0.03(1)	0.17(8)	0.26(0)

for the extrapolation, which gives an upper bound for the bond strengths. The data can also be fitted using a power-law function:

$$I_{ij}^{(ab)}(L) = I_{ij}^{(ab)} + A/L^B, \tag{20}$$

where $I_{ij}^{(ab)}$, A, and B are free parameters. The residual sum of squares is roughly of the same order of magnitude for both types of fits, $O(10^{-6})$, therefore we give the values of the order parameters for both fits in Table II. The quadratic extrapolation clearly overestimates the order parameters while the polynomial fit underestimates it, since we expect that the order parameter begins to saturate as soon as the bulk limit is achieved.

The other order parameter defined in Eq. (19) is shown in Fig. 8 for $J/U = 0.1$ and $J/U = 0.3$. The extrapolations using the two different fits are shown in Table II. From these calculations we conclude that the intermediate phase remains dimerized in the thermodynamic limit, which is a clear sign of spontaneous symmetry breaking. Moreover, it is a surprising phenomenon, since dimerization has not been observed at all in the periodic Anderson model without the Hund's coupling.

Now we return to the entanglement patterns in Fig. 6. We consider first the entanglement between localized electrons by examining $\rho^{(ff)}_{L/2-1,L/2}$ and $\rho^{(ff)}_{L/2,L/2+1}$ for $L = 16$. We have seen that due to the finite-size effects the strengths of the bonds change, but the qualitative picture, which can be obtained from the analysis of the density matrices, remains. For $\rho^{(ff)}_{L/2-1,L/2}$ one of the eigenvalues is larger by an order of magnitude than

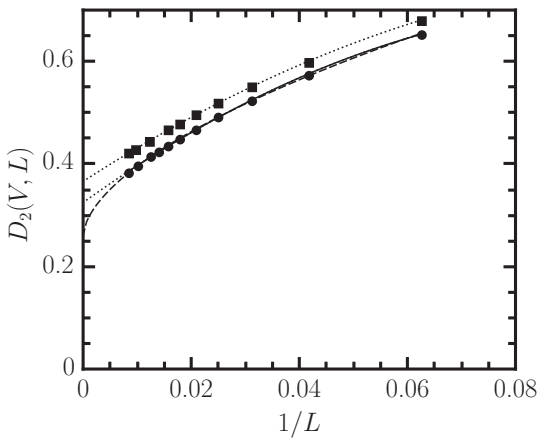

FIG. 8. Finite-size scaling of the order parameter in Eq. (19). The symbols •, ■ belong to $V/W = 0.569$, $J/U = 0.1$ and $V/W = 1.665$, $J/U = 0.3$, respectively. The dotted and dashed lines denote the quadratic and power-law fits, respectively.

the others, and the corresponding eigenfunction is

$$\phi^{(ff)}_{L/2-1,L/2} = 0.7071\left(|\uparrow\rangle^{(f)}_{L/2-1}|\downarrow\rangle^{(f)}_{L/2} - |\downarrow\rangle^{(f)}_{L/2-1}|\uparrow\rangle^{(f)}_{L/2}\right) + 0.006\left(|\uparrow\downarrow\rangle^{(f)}_{L/2-1}|0\rangle^{(f)}_{L/2} + |0\rangle^{(f)}_{L/2-1}|\uparrow\downarrow\rangle^{(f)}_{L/2}\right), \tag{21}$$

which means that the origin of the strong entanglement between localized electrons on neighboring sites is the singlet formation. If we consider the neighboring bond, we obtain from $\rho^{(ff)}_{L/2,L/2+1}$ that one of the eigenvalues is $\omega_1 = 0.3953$ and there is a threefold degenerate eigenvalue $\omega_2 = 0.1500$. The eigenvector corresponding to the former one is essentially the same as in Eq. (21), while the eigenvectors corresponding to the latter one are the triplet components described in (15). Due to the fact that triplet components are mixed with a larger weight to the singlet component, it destroys the singlet bond between the localized electrons resulting in a much weaker entanglement. Qualitatively the above considerations remain valid for the explanation of entanglement between the itinerant electrons. Lastly we examine the entanglement within a site with the help of $\rho^{(cf)}_{L/2,L/2}$. In this case we have again a nondegenerate eigenvalue $\omega_1 = 0.2467$, and a threefold degenerate one $\omega_2 = 0.2274$. The eigenvector corresponding to ω_1 is

$$\phi^{(cf)}_{L/2,L/2} = 0.5885\left(|\uparrow\rangle^{(c)}_{L/2}|\downarrow\rangle^{(f)}_{L/2} - |\downarrow\rangle^{(c)}_{L/2}|\uparrow\rangle^{(f)}_{L/2}\right) + 0.3921\left(|\uparrow\downarrow\rangle^{(c)}_{L/2}|0\rangle^{(f)}_{L/2} + |0\rangle^{(c)}_{L/2}|\uparrow\downarrow\rangle^{(f)}_{L/2}\right), \tag{22}$$

while the eigenvectors of ω_2 are the triplet states in (15). It can be seen easily that the on-site spin correlation is still ferromagnetic, but significantly reduced compared to the Haldane-like phase. While the on-site singlet state has negligible weight in the Haldane-like phase, in the dimerized state the on-site triplet and singlet states are mixed with comparable weights.

D. Discussion

In the light of the above results it is worth examining the nature of the phase transitions and comparing the properties of the phases to what has been obtained in infinite dimensions.

As we mentioned, there is no phase transition when $J = 0$, where the ground state is Kondo-singlet-like discussed in Sec. III. A. For any finite J two new phases appear, namely a Haldane-like and a dimerized phase whose properties are discussed below, and they disappear as $J \to 0$.

We have seen that for $V < V_1^{\rm cr}$ the ground state is Haldane-like while for $V > V_2^{\rm cr}$ Kondo-singlet-like, and both are gapful and homogeneous. For $V_1^{\rm cr} < V < V_2^{\rm cr}$ the translational symmetry is broken due to the dimerization. It is worth noting that a similar phase diagram has been obtained in frustrated spin ladders [53], where on-site and nearest-neighbor antiferromagnetic couplings compete with each other.

The existence of different phases can be corroborated by investigating the entanglement spectrum [54] which is known to be a useful tool to detect symmetry-protected topological order [55]. It is obtained from the eigenvalues (Λ_i) of the density matrix of a half chain. In the Haldane-like phase the degeneracy of each eigenvalue is an even number [55], while both even and odd degeneracies may appear in other

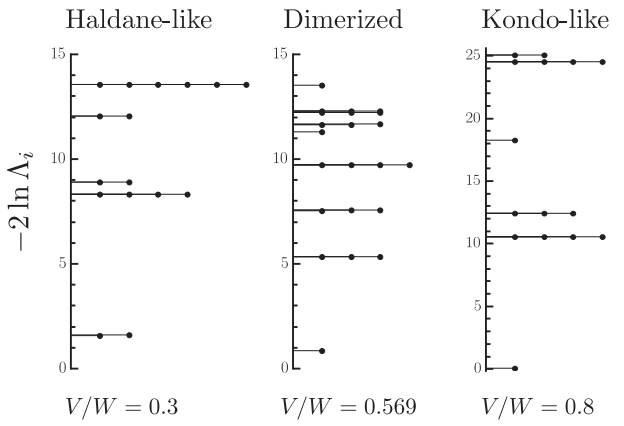

FIG. 9. The entanglement spectrum in the three different phases for $J/U = 0.1$ and $L = 120$ (for better visibility only the lower part is shown).

phases. For short chains both even and odd degeneracies occur for any V/W. This picture drastically changes for longer chains, namely for $L > 90$. Here the correlation between the end spins suddenly vanishes, which is marked by a jump in the block entropy for small V/W. While even and odd degeneracies remain in the spectrum for $V > V_1^{\rm cr}$, the entanglement spectrum contains nearly degenerate eigenvalues whose multiplicity is even for $V < V_1^{\rm cr}$. In the thermodynamic limit the eigenvalues becomes exactly degenerate. In Fig. 9 the low-lying eigenvalues and their degeneracies are shown with a logarithmic scale corresponding to the three different phases for $L = 120$. While the spectra of the dimerized and Kondo-like phases contain eigenvalues with odd and even degeneracy, only even degeneracy is present in the Haldane-like phase in agreement with our expectation.

It is interesting to compare these findings with what has been obtained by DMFT [27]. Surprisingly, three distinct phases appear also in the DMFT phase diagram, although their properties are significantly different. In DMFT there is a phase with antiferromagnetic long-range order in which the on-site spins are coupled ferromagnetically while the nearest-neighbor coupling is antiferromagnetic (AF I phase). Further increase of the hybridization drives the system into an intermediate phase ($V_1^{\rm cr} < V < V_2^{\rm cr}$) where another type of antiferromagnetic order takes place. Here the on-site coupling becomes antiferromagnetic, while the nearest-neighbor coupling remains antiferromagnetic (AF II phase). Finally, for $V_2^{\rm cr} < V$ Kondo-like behavior is realized.

In one dimension we cannot expect true long-range magnetic order, only slow decay of the correlation functions. For $V < V_1^{\rm cr}$ the on-site spins are parallel due to the strong Hund's coupling. This Haldane-like phase might be the residue of the AF I ordered phase obtained in the DMFT calculation. Above the second critical point, $V_2^{\rm cr} < V$, the ground state is homogeneous, and strong on-site correlations appear, which originate from the enhanced Kondo effect and the sites are occupied more and more by two localized or delocalized electrons or vice versa. The properties of the Kondo phase are consistent with what has been obtained in DMFT. Both methods exhibit an intermediate phase between them, however, their properties are completely different, which is caused by the enhanced quantum fluctuations. The appearance of the dimerized phase may originate from the competition between the Haldane-like and Kondo singlet phase. This may not surprise us if we recall that dimerization has been found in a two-component system via a purely electronic mechanism [56]. The present case is similar although for antiferromagnetic interactions between localized electrons.

IV. CONCLUSIONS

We investigated an extended periodic Anderson model in one dimension to understand the role of the Hund's coupling between itinerant and localized electrons. We carried out accurate DMRG calculations with quantum information loss $\chi = 3 \times 10^{-6}$ up to the accessible chain length $L = 120$. For such error margin we found that the two competing processes, the Hund's coupling and the Kondo effect, lead to the appearance of two new nontrivial phases. The enhanced quantum fluctuations in one dimension crucially affects the properties of the phases obtained in infinite spatial dimensions. We performed a quantum information analysis and determined the entanglement spectrum in the various phases and the entanglement patterns between the system components. Moreover, using the eigensystem of the two-site density matrices we examined what physical processes lead to the development of entanglement. We found that for $V < V_1^{\rm cr}$ the itinerant and localized electrons form a local triplet within a site and couple to the nearest-neighbor sites antiferromagnetically. Here the model can be considered as an $S = 1$ spin chain with antiferromagnetic coupling and we have a Haldane-like ground state. This is also corroborated by the entanglement spectrum. For $V_1^{\rm cr} < V < V_2^{\rm cr}$ we have an intermediate dimerized phase, in which strong and weak singlet bonds alternate between nearest-neighbor itinerant and localized electrons. We have seen that the region where dimerization occurs expands as the Hund's coupling is increased and shifts to large values of the hybridization. Finally, for $V > V_2^{\rm cr}$ the ground state is homogeneous, and local singlets are formed at each site either by two localized/conduction electrons or by a localized and an itinerant electron.

ACKNOWLEDGMENT

This work was supported in part by the Hungarian Research Fund (OTKA) through Grants No. K 100908 and No. NN110360.

[1] S. Jin, T. H. Tiefel, M. McCormack, R. A. Fastnacht, R. Ramesh, and L. H. Chen, Science **264**, 413 (1994).

[2] A. P. Ramirez, J. Phys.: Condens. Matter **9**, 8171 (1997).

[3] Y.-K. Liu, Y.-W. Yin, and X.-G. Li, Chin. Phys. B **22**, 087502 (2013).
[4] Y. Tomioka, A. Asamitsu, Y. Moritomo, H. Kuwahara, and Y. Tokura, Phys. Rev. Lett. **74**, 5108 (1995).
[5] S. Nakatsuji and Y. Maeno, Phys. Rev. Lett. **84**, 2666 (2000).
[6] V. I. Anisimov, I. A. Nekrasov, D. E. Kondakov, T. M. Rice, and M. Sigrist, Eur. Phys. J. B **25**, 191 (2002).
[7] S. Nakatsuji, D. Hall, L. Balicas, Z. Fisk, K. Sugahara, M. Yoshioka, and Y. Maeno, Phys. Rev. Lett. **90**, 137202 (2003).
[8] A. Koga, N. Kawakami, T. M. Rice, and M. Sigrist, Phys. Rev. Lett. **92**, 216402 (2004).
[9] A. Koga, K. Inaba, and N. Kawakami, Prog. Theor. Phys. Suppl. **160**, 253 (2005).
[10] A. Koga, N. Kawakami, T. M. Rice, and M. Sigrist, Phys. Rev. B **72**, 045128 (2005).
[11] J. Bünemann, D. Rasch, and F. Gebhard, J. Phys.: Condens. Matter **19**, 436206 (2007).
[12] L. de'Medici, A. Georges, and S. Biermann, Phys. Rev. B **72**, 205124 (2005).
[13] P. Fulde, J. Keller, and G. Zwicknagl, in *Solid State Physics: Advances in Research and Applications*, edited by H. Ehrenreich and D. Turnbull (Academic Press, San Diego, 1988), Vol. 41, pp. 1–150.
[14] A. C. Hewson, *The Kondo Problem to Heavy Fermions* (Cambridge University Press, Cambridge, 1993).
[15] P. Fazekas, *Lecture Notes on Electron Correlation and Magnetism* (World Scientific, Singapore, 1999).
[16] E. A. Winograd and L. de' Medici, Phys. Rev. B **89**, 085127 (2014).
[17] A. M. Oleś, Phys. Rev. B **28**, 327 (1983).
[18] T. Schork and S. Blawid, Phys. Rev. B **56**, 6559 (1997).
[19] T. Yoshida, T. Ohashi, and N. Kawakami, J. Phys. Soc. Jpn. **80**, 064710 (2011).
[20] I. Hagymási, K. Itai, and J. Sólyom, Phys. Rev. B **85**, 235116 (2012).
[21] K. Miyake, J. Phys.: Condens. Matter **19**, 125201 (2007).
[22] S. Watanabe, M. Imada, and K. Miyake, J. Phys. Soc. Jpn. **75**, 043710 (2006).
[23] I. Hagymási, K. Itai, and J. Sólyom, Phys. Rev. B **87**, 125146 (2013).
[24] T. Yoshida and N. Kawakami, Phys. Rev. B **85**, 235148 (2012).
[25] I. Hagymási, J. Sólyom, and Ö. Legeza, Phys. Rev. B **90**, 125137 (2014).
[26] A. Koga, N. Kawakami, R. Peters, and T. Pruschke, Phys. Rev. B **77**, 045120 (2008).
[27] A. Koga, N. Kawakami, R. Peters, and T. Pruschke, J. Phys. Soc. Jpn. **77**, 033704 (2008).
[28] C. M. Varma and A. Zawadowski, Phys. Rev. B **32**, 7399 (1985).
[29] K. Penc and J. Sólyom, Phys. Rev. B **41**, 704 (1990).
[30] S. R. White, Phys. Rev. Lett. **69**, 2863 (1992).
[31] S. R. White, Phys. Rev. B **48**, 10345 (1993).
[32] U. Schollwöck, Rev. Mod. Phys. **77**, 259 (2005).
[33] R. M. Noack and S. R. Manmana, AIP Conf. Proc. **789**, 93 (2005).
[34] K. Hallberg, Adv. Phys. **55**, 477 (2006).
[35] Ö. Legeza and J. Sólyom, Phys. Rev. B **68**, 195116 (2003).
[36] G. Vidal, J. I. Latorre, E. Rico, and A. Kitaev, Phys. Rev. Lett. **90**, 227902 (2003).
[37] P. Calabrese and J. Cardy, J. Stat. Mech. (2004) P06002.
[38] J. Rissler, R. M. Noack, and S. R. White, Chem. Phys. **323**, 519 (2006).
[39] Ö. Legeza and J. Sólyom, Phys. Rev. Lett. **96**, 116401 (2006).
[40] L. Amico, R. Fazio, A. Osterloh, and V. Vedral, Rev. Mod. Phys. **80**, 517 (2008).
[41] S.-J. Gu, S.-S. Deng, Y.-Q. Li, and H.-Q. Lin, Phys. Rev. Lett. **93**, 086402 (2004).
[42] L.-A. Wu, M. S. Sarandy, and D. A. Lidar, Phys. Rev. Lett. **93**, 250404 (2004).
[43] M.-F. Yang, Phys. Rev. A **71**, 030302 (2005).
[44] S.-S. Deng, S.-J. Gu, and H.-Q. Lin, Phys. Rev. B **74**, 045103 (2006).
[45] Ö. Legeza, J. Röder, and B. A. Hess, Phys. Rev. B **67**, 125114 (2003).
[46] Ö. Legeza and J. Sólyom, Phys. Rev. B **70**, 205118 (2004).
[47] G. Barcza, Ö. Legeza, K. H. Marti, and M. Reiher, Phys. Rev. A **83**, 012508 (2011).
[48] K. Boguslawski, P. Tecmer, G. Barcza, Ö. Legeza, and M. Reiher, J. Chem. Theory Comp. **9**, 2959 (2013).
[49] M. M. Wolf, F. Verstraete, M. B. Hastings, and J. I. Cirac, Phys. Rev. Lett. **100**, 070502 (2008).
[50] S. Furukawa, V. Pasquier, and J. Shiraishi, Phys. Rev. Lett. **102**, 170602 (2009).
[51] G. Barcza, R. M. Noack, J. Sólyom, and Ö. Legeza, arXiv:1406.6643.
[52] S. R. White and D. A. Huse, Phys. Rev. B **48**, 3844 (1993).
[53] E. H. Kim, Ö. Legeza, and J. Sólyom, Phys. Rev. B **77**, 205121 (2008).
[54] H. Li and F. D. M. Haldane, Phys. Rev. Lett. **101**, 010504 (2008).
[55] F. Pollmann, A. M. Turner, E. Berg, and M. Oshikawa, Phys. Rev. B **81**, 064439 (2010).
[56] J. Sirker, A. Herzog, A. M. Oleś, and P. Horsch, Phys. Rev. Lett. **101**, 157204 (2008).